A Ka-band Celestial Reference Frame with Applications to Deep Space Navigation

Christopher S. Jacobs
Jet Propulsion Laboratory, California Institute of Technology, 4800 Oak Grove Dr., Pasadena, CA 91109, (818)354-7490, (818)393-4965, Christopher.S.Jacobs@jpl.nasa.gov
J. Eric Clark
Jet Propulsion Laboratory, California Institute of Technology, 4800 Oak Grove Dr., Pasadena, CA 91109, (818)393-5994, (818)393-4965, John.E.Clark@jpl.nasa.gov
Cristina Garcia-Miro
Ingenieria y Servicios Aeroespaciales, Madrid Deep Space Communications Complex, Paseo del Pintor Rosales, 34 bajo, E-28008, Madrid, Spain, 34 91 867 7130, fax: n/a, cgmiro@mdscc.nasa.gov
Shinji Horiuchi
C.S.I.R.O. Astronomy and Space Science/NASA, Canberra Deep Space Communications Complex, P.O. Box 1035, AU Tuggeranong ACT 2901, Australia, 61 02 6201 7800, fax: n/a, shoriuchi@cdscc.nasa.gov
Ioana Sotuela
Ingenieria y Servicios Aeroespaciales, Madrid Deep Space Communications Complex, Paseo del Pintor Rosales, 34 bajo, E-28008, Madrid, Spain, 34 91 867 7207, fax: n/a, isotuela@mdscc.nasa.gov

Abstract

The Ka-band radio spectrum is now being used for a wide variety of applications. This paper highlights the use of Ka-band as a frequency for precise deep space navigation based on a set of reference beacons provided by extragalactic quasars which emit broadband noise at Ka-band.

This quasar-based celestial reference frame is constructed using X/Ka-band (8.4/32 GHz) from fifty-five 24-hour sessions with the Deep Space Network antennas in California, Australia, and Spain. We report on observations which have detected 464 sources covering the full 24 hours of Right Ascension and declinations down to −45 deg. Comparison of this X/Ka-band frame to the international standard S/X-band (2.3/8.4 GHz) ICRF2 shows wRMS agreement of ~200 micro-arcsec (μas) in α cos δ and ~300 μas in δ. There is evidence for systematic errors at the 100 μas level. Known errors include limited SNR, lack of instrumental phase calibration, tropospheric refraction mis-modeling, and limited southern geometry. The motivation for extending the celestial reference frame to frequencies above 8 GHz is to access more compact source morphology for improved frame stability and to support spacecraft navigation for Ka-band based NASA missions.

1. Introduction

For over three decades now, radio frequency work in deep space navigation as well as in global astrometry and geodesy has been done at S-band (2.3 GHz) and X-band (8.4 GHz). While this work has been tremendously successful in producing 100 μas level global astrometry (*e.g.* Ma et al, 2009) and sub-cm geodesy, developments made over the last decade have made it possible to consider the merits of moving to a new set of frequencies. This paper will discuss the construction of a celestial

reference frame at X/Ka-band (8.4/32 GHz)[1] for deep space navigation based on Very Long Baseline Interferometry (VLBI) observations. What are the pros and cons of moving from X-band to Ka-band?

Advantages: Moving the observing frequencies up by approximately a factor of four has several advantages—enough that Ka-band will be mandatory on all deep space missions beyond 2016. For NASA's Deep Space Network, the driver is the potential for higher data rates for telemetry signals from deep space probes. Advantages include:

1) Improved telemetry rates to deep space probes by as much as 8 dB (Koerner, 1986; Slobin *et al*, 1987)

2) Potential for more accurate spacecraft tracking measurements as demonstrated with the Mars 2005 mission (Shambayati *et al*, 2006)

3) spatial distribution of flux becomes significantly more compact (Charlot et al, 2010) lending hope that the positions will be more stable over time

4) Radio Frequency Interference (RFI) at S-band would be avoided

5) Ionosphere and solar plasma effects on group delay are reduced by a factor of ~15!

6) Spacecraft component size and mass scale down with wavelength.

Disadvantages: While the above items are very significant advantages, they do not come without a price. The change from 2.3 / 8.4 GHz to 8.4 / 32 GHz moves one closer to the water line at 22 GHz and thus increases the system temperature from a few Kelvins per atmospheric thickness up to 10--15 Kelvins per atmosphere or more. Thus one becomes much more sensitive to weather. Furthermore, the sources themselves are in general weaker and many sources are resolved. Also, with the observing wavelengths shortened by a factor of 4, the coherence times are shortened so that practical integration times are a few minutes or less---even in relatively dry climates. The shorter wavelengths also imply that the antenna pointing accuracy requirements must be tightened by the same factor of 4.

The combined effect of these disadvantages is to lower the system sensitivity. Fortunately, advances in recent years in recording technology make it feasible and affordable to offset these losses in sensitivity by recording more bits. Thus while most of the X/Ka data presented in this paper used the same overall 112 Mbps bit rate as previous S/X work, recent data were taken at 448 Mbps with an increase to 2048 Mbps hoped for within the next year or two.

This paper is organized as follows: We will describe the observations, modeling, and present the results. Next, we will estimate the accuracy by comparing to the S/X-based ICRF2 (Ma et al, 2009) including a look at zonal errors. This will be complemented by a discussion of the error budget and the potential for improving the geometry of our network by adding a southern station. Lastly, we will discuss the potential for linking the X/Ka radio frame to the optical frame expected to be produced by ESA's Gaia mission.

2. Observations

The results presented here are from fifty-five Very Long Baseline Interferometry (VLBI) observing sessions of ~24 hour duration done from July 2005 until June 2011 using NASA's Deep Space Stations (DSS) 25 or DSS 26 in Goldstone, California to either DSS 34 in Tidbinbilla, Australia or DSS 54 or DSS 55 outside Madrid, Spain to form interferometric baselines of 10,500 and 8,400 km length, respectively.

[1] In VLBI practice, the juxtaposition of two frequency bands is a convention in which lower frequency band is being used for plasma calibration while the higher band is the principal source of the angular coordinate measurement.

We recorded VLBI data simultaneously at X-band (8.4 GHz) and Ka-band (32 GHz). Initially, sampling of each band was at 56 Mbps while more recent passes used 160/288 Mbps at X/Ka. Each band used a spanned bandwidth of 360 MHz. The data were filtered, sampled, and recorded to the Mark4 or Mark5A VLBI systems. The data were then correlated with the JPL BlockII correlator (O'Connor, 1987) or the JPL SOFTC software correlator (Lowe, 2005). Fringe fitting was done with the FIT fringe fitting software (Lowe, 1992). The measurements covered the full 24 hours of Right Ascension and declinations down to -45 deg. Individual observations were about 1 to 2 minutes in duration.

3. Modelling

The above described set of observations were then modelled using the MODEST software (Sovers, Fanselow, & Jacobs, 1998). Nutation was modelled with the MHB nutation model (Mathews *et al*, 2002) augmented by sub-mas empirical corrections from S/X VLBI analysis for free core nutation and decadal scale effects. We used the empirically determined UT1-UTC and Polar Motion of JPL's "Space" series (Ratcliff & Gross, 2010). The celestial frame was aligned to the ICRF2 defining sources (Ma, *et al*, 2009) using a no-net-rotation constraint (Jacobs *et al*, 2010). Station velocities were estimated; station locations were estimated with a 2 cm constraint per component to a decades-long S/X-band VLBI solution.

4. Results

In all, we detected 464 extragalactic radio sources which covered the full 24 hours of Right Ascension (RA) and Declinations down to -45 deg. Figs. 1a,b plot these sources using Hammer's (1892) equal-area projection to show their distribution over the sky. RA=0 is at the center. The ecliptic plane is shown by the sinusoidal-shaped curve and the Galactic plane is indicated by the Omega-shaped curve. The source symbols indicate the 1-sigma formal RA and declination uncertainties with the value ranges indicated in the figure's legend.

Note that the declination precision drops as one moves toward the south. This is a result of having significantly less data on the California to Australia baseline combined with the need to observe sources closer to the horizon as declination moves south, thus incurring greater error from higher system temperatures.

5.1 Accuracy Estimate Based on Comparison to ICRF2

Experience shows that formal uncertainties tend to underestimate true errors. An independent estimate of position errors was obtained by comparing our X/Ka-band positions to the S/X-based ICRF2. For 428 common, well observed sources, the weighted RMS (wRMS) differences of X/Ka minus S/X are 203 μas in α cos δ and 312 μas in δ.

5.2. Zonal Errors

The Section 5.1 gave a measure of overall coordinate agreement. We now turn to X/Ka - S/X differences which are systematically correlated as a function of position on the sky. The slopes of $\Delta\alpha\ \cos(\delta)$ and $\Delta\delta$ vs. α and δ are given in Table 1 to the right. The most significant is $\Delta\alpha\ \cos(\delta)$ vs. α at 1.6 sigma. Note that the use of full correlations had a significant effect on the determination of these slopes.

Δα cos δ vs. α	2.6 +- 1.6 μas/hr
Δδ vs. α	0.9 +- 1.1 μas/hr
Δα cos δ vs. δ	0.5 +- 0.5 μas/deg
Δδ vs. δ	0.5 +- 0.9 μas/deg

Table 1. Slope of coordinate differences

Figs. 2a,b show in detail $\Delta\alpha\ \cos\delta$ vs. δ and $\Delta\delta$ vs. δ for XKa - ICRF2.

5.3. Discussion of the Error Budget

Having assessed the accuracy of the X/Ka coordinates using the much larger ICRF2 S/X data set as the standard of accuracy, we now discuss the major contributions to the errors in the X/Ka measurements: SNR, instrumentation, and troposphere. Examining the weighted RMS group delay vs. the Ka-band SNR revealed that for SNR < 15 dB, the thermal error dominates the error budget. For higher SNRs, troposphere and instrumentation errors become more important. Binning of wRMS delay vs. airmass thickness shows that troposphere is not the dominant error due to the generally low SNRs just mentioned. However, the phase rates (which carry much less weight in the fit) are dominated by errors from tropospheric mismodelling, thus hinting that troposphere will become more important as our SNR improves with increased data rates.

Lastly, we have errors from un-calibrated instrumentation. A proto-type phase calibrator has been developed in order to calibrate the signal path from the feed to the sampler (Hammel *et al*, 2003). Test data indicate an approximately diurnal instrumental effect with ~180 psec (5.4cm) RMS. Although the data themselves can be used to estimate instrumental parameters which partially characterize this effect, operational phase calibrators are being built in order to make direct reliable calibrations of the instrumentation.

6. Southern Geometry

The Besides the three classes of measurement errors described above, our reference frame suffers from a very limited geometry--we have only one station in the southern hemisphere. In order to better understand this limitation, we simulated the effect of adding a second southern station (Bourda *et al*, 2010). In this simulation, data from the first 50 real X/Ka sessions (Fig. 3a: 415 sources) were augmented by simulated data for 1000 group delays each with SNR = 50 from a 9000 km baseline: Australia to S. America or S. Africa. Fig. 3b shows the frame augmented with simulated data.

The augmented frame extends declination coverage to the south polar cap region: -45 to -90 deg. Precision in the south cap region was ~200 μas (1 nrad) and in the mid south precision was 200 to 1000 μas, all with just a few days observing. We conclude that adding a second southern station would greatly aid our X/Ka frame's accuracy. In fact, the resulting four station network should compete well in astrometric accuracy with the historical S/X network and its international standard ICRF2. Fig. 4 shows the full set of candidates for further X/Ka observations (Sotuela *et al*, 2011).

7. Potential Frame tie to the Gaia optical Frame

The Gaia mission (2012 launch) is expected to measure 10^9 objects with tens of μas precision including 500,000 quasars of which ~2000 are expected to be both optically bright (V < 18 mag) and radio loud (30 to 300+ milli-Jansky). We have 336 sources with optical counterparts (Veron-Cetty & Veron, 2010) with visual (500 to 600 nm) magnitude, V, bright enough to be detected by Gaia (V< 20 mag). Of these, 130 are bright by Gaia standards (V < 18 mag).

Using existing X/Ka-band position uncertainties and simulated Gaia uncertainties (corrected for ecliptic latitude, but not V-I color), we did a covariance study of the 3-D rotation between the X/Ka and Gaia frames resulting in formal uncertainties of 16, 13, and 11 μas (1-sigma) in the 3 Cartesian rotations R(x,y,z), respectively

Description	Magnitude range	Number	Percent
Bright	0 < V < 18	130	29%
Detectable	18 < V < 20	206	45%
Undetectable	20 < V	51	11%
Unmeasured	unknown	68	15%

Table 2. Optical magnitude ranges of sources

(Jacobs *et al*, 2011). The result is dominated by X/Ka uncertainties which have potential for a factor of two or more improvement by the time of the final Gaia catalog in 2021. Thus a frame tie precision of 5 to 10 μas (25 to 50 pico-radian) may eventually be possible.

8. Conclusion

We have demonstrated that Ka-band radio observations can be used to construct a high accuracy celestial reference frame for use in deep space navigation. Our X/Ka-band (8.4/32 GHz) frame has 464 sources detected with Very Long Baseline Interferometry (VLBI). For the 428 sources common to our X/Ka frame and the S/X-based ICRF2, we find positional agreement of 203 μas (1nrad) in Right Ascension (arc) and 312 μas (1.5 nrad) in declination with zonal errors of 100 μas (0.5 nrad). Improvements in data rates and instrumental calibration are projected to allow better than 200 μas (1 nrad) accuracy within the next few years. Simulations of adding another southern station predict better than 200 μas for the southern polar cap within a very short time of adding data from an all southern baseline. This gives hope that better than 100 μas accuracy over the full sky might be achieved within a few years of adding such a southern baseline.

Lastly, simulations of the X/Ka sources with identified optical counterparts bright enough to be detected by ESA's Gaia mission show potential for a frame tie with 5 to 15 μas precision and reduced systematic errors from source structure and core shift compared to S/X-band. All of these things demonstrate the value of Ka-band for deep space navigation work.

Acknowledgements: The research described herein was performed at the Jet Propulsion Laboratory of the California Institute of Technology under contract with the National Aeronautics and Space Administration. Government sponsorship acknowledged.

References

1 Bourda *et al*, Proc. ELSA Conference: Gaia at the Frontiers of Astrometry, Sevres, France, (2010). ftphip.obspm.fr/gaia2010/IMG/pdf/Poster_Bourda.pdf

2 Charlot *et al*, AJ, 139, 5, (2010), p. 1713. doi: 10.1088/0004-6256/139/5/1713

3 Hamel *et al*, NASA JPL IPN Prog. Report, 42-154, (2003), pp. 1-14. http://tmo.jpl.nasa.gov/progress_report/42-154/154H.pdf

4 Hammer, Petermanns Mitt., 38, (1892), pp. 85-87.

5 Jacobs *et al*, IVS 2010 Gen. Meeting Proc., eds. D. Behrend & K. D. Baver, NASA/CP-2010, IVS Analysis Session, Hobart, Tasmania, Australia, (2010). ftp://ivscc.gsfc.nasa.gov/pub/general-meeting/2010/presentations/GM2010_AW_jacobs.pdf

6 Jacobs *et al*, Proc. 20th EVGA, Bonn, Germany, (2011). http://www.mpifr-bonn.mpg.de/div/meetings/20thEVGA/EVGA-Talks/Jacobs_XKa_110330.pdf

7 Koerner, NASA IPN Progress Report, 42-87, (1986) pp. 65-80. http://tmo.jpl.nasa.gov/progress report/42- 87/87H.PDF

8 Lowe, *Theory of Post-BlockII VLBI Observable Extraction*, JPL Pub. 92-7, Pasadena CA, (1992). http://ntrs.nasa.gov/archive/nasa/casi.ntrs.nasa.gov/19940009399_1994009399.pdf

9 Lowe, *SOFTC: A Software VLBI Correlator*, JPL sec. 335, Pasadena, CA, (2005).

10 Ma, *et al,* editors: Fey, Gordon Jacobs, *IERS Tech Note 35*, IERS, Frankfurt, Germany, (2009). http://www.iers.org/nn_11216/IERS/EN/Publications/TechnicalNotes/tn35.html

11 Mathews, Herring, and Buffet, JGR, 107, B4, 10.1029/2001JB000390, (2002).
http://www.agu.org/journals/jb/jb0204/2001JB000390/

12 O'Connor, *Introduction to the BlockII Correlator hardware*, JPL, Pasadena CA, (1987).

13 Ratcliff and Gross, JPL Publication 10-4, Pasadena CA, (2010).
http://hdl.handle.net/2014/41512

14 Shambayati *et al*, Proc. AIAA 9th Int. Conf. Space Operations, (2006).
http://trs-new.jpl.nasa.gov/dspace/bitstream/2014/39654/1/06-0902.pdf

15 Slobin *et al*, NASA JPL IPN Progress Report, 42-88, (1987) pp. 135-140.
http://tmo.jpl.nasa.gov/progress report/42- 88/88R.PDF

16 Sotuela *et al*, GREAT-ESF workshop, Porto, Portugal, (2011).
http://www.fc.up.pt/great-ws-porto/program.html

17 Sovers, Fanselow, and Jacobs, Rev. Mod. Phys., 70, 4, (1998), pp.1393-1454.
doi: 10.1103/RevModPhys.70.1393

18 Veron-Cetty & Veron, (13th ed.), A&A, 51, (2010).
vizier.cfa.harvard.edu/viz-bin/VizieR?-source=VII/258

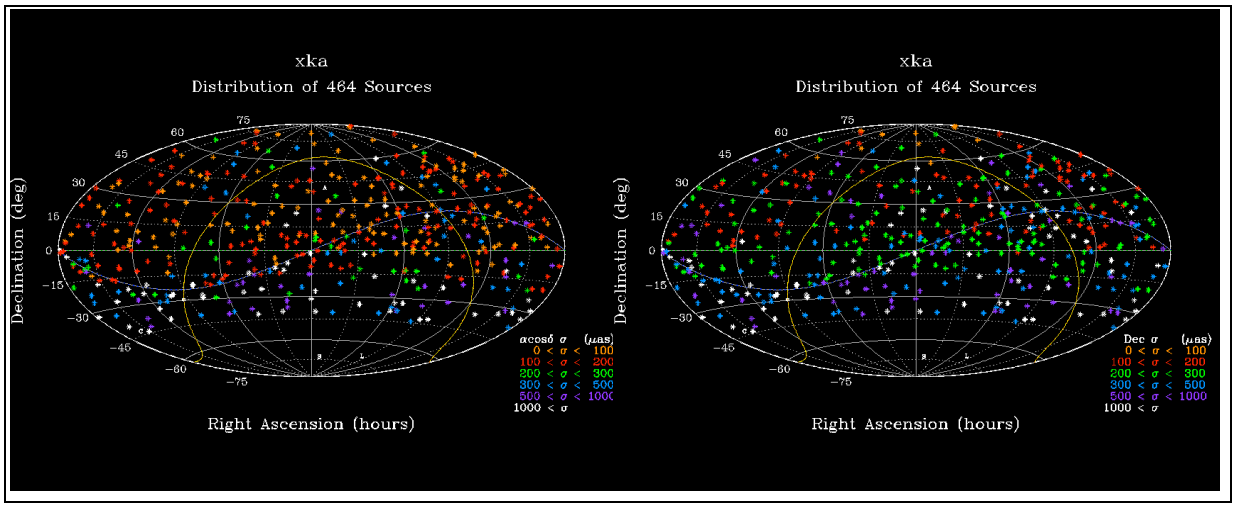

Fig. 1a Right Ascension uncertainties

Fig.1b Declination Uncertainties

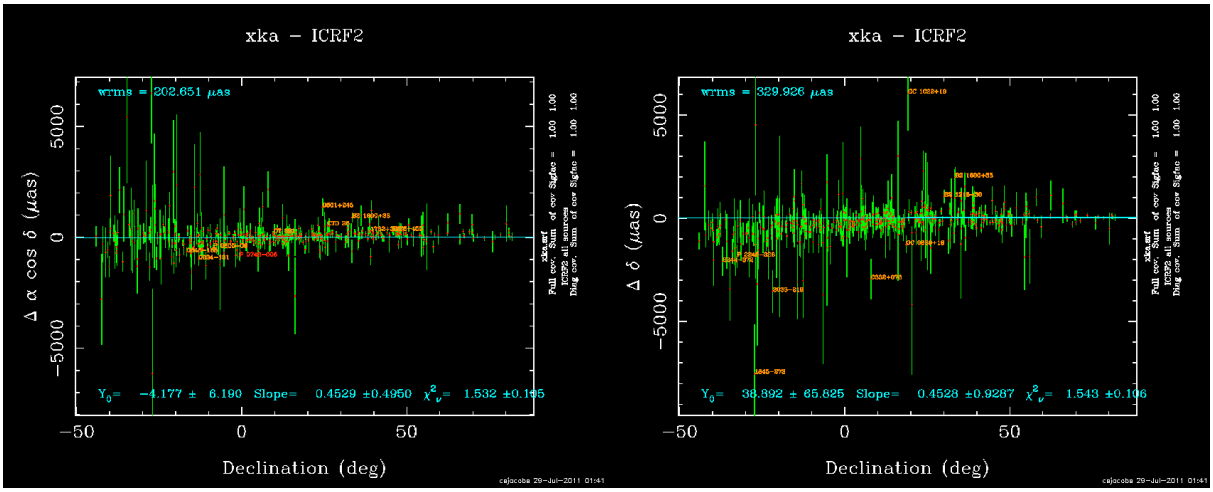

Fig. 2a. X/Ka-ICRF2: $\Delta\alpha\cos\delta$

Fig. 2b X/Ka-ICRF2: $\Delta\delta$ **vs.** δ

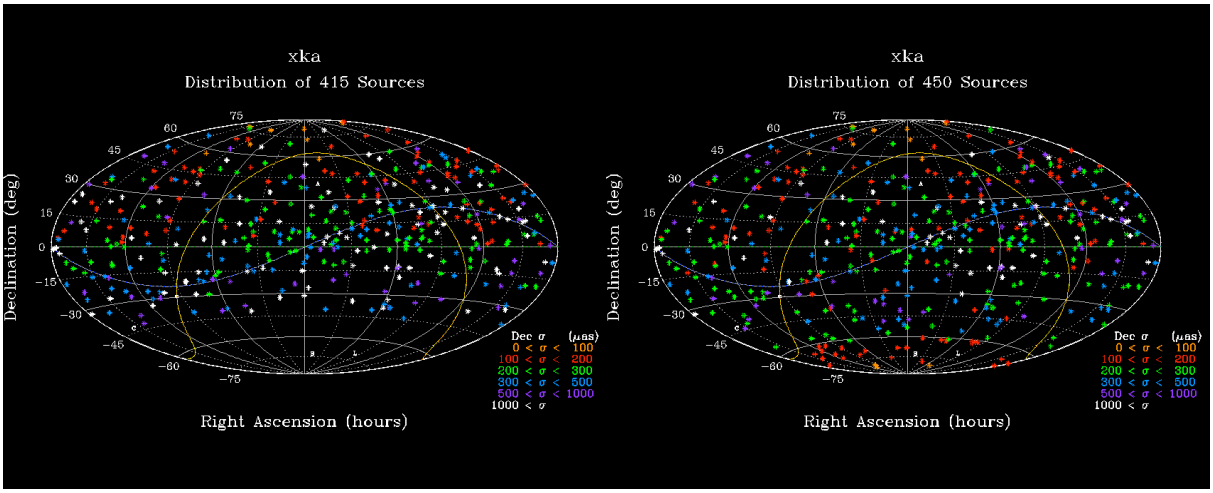

Fig. 3a X/Ka real data (after 50 sessions)

Fig. 3b Real data + simulated southern baseline

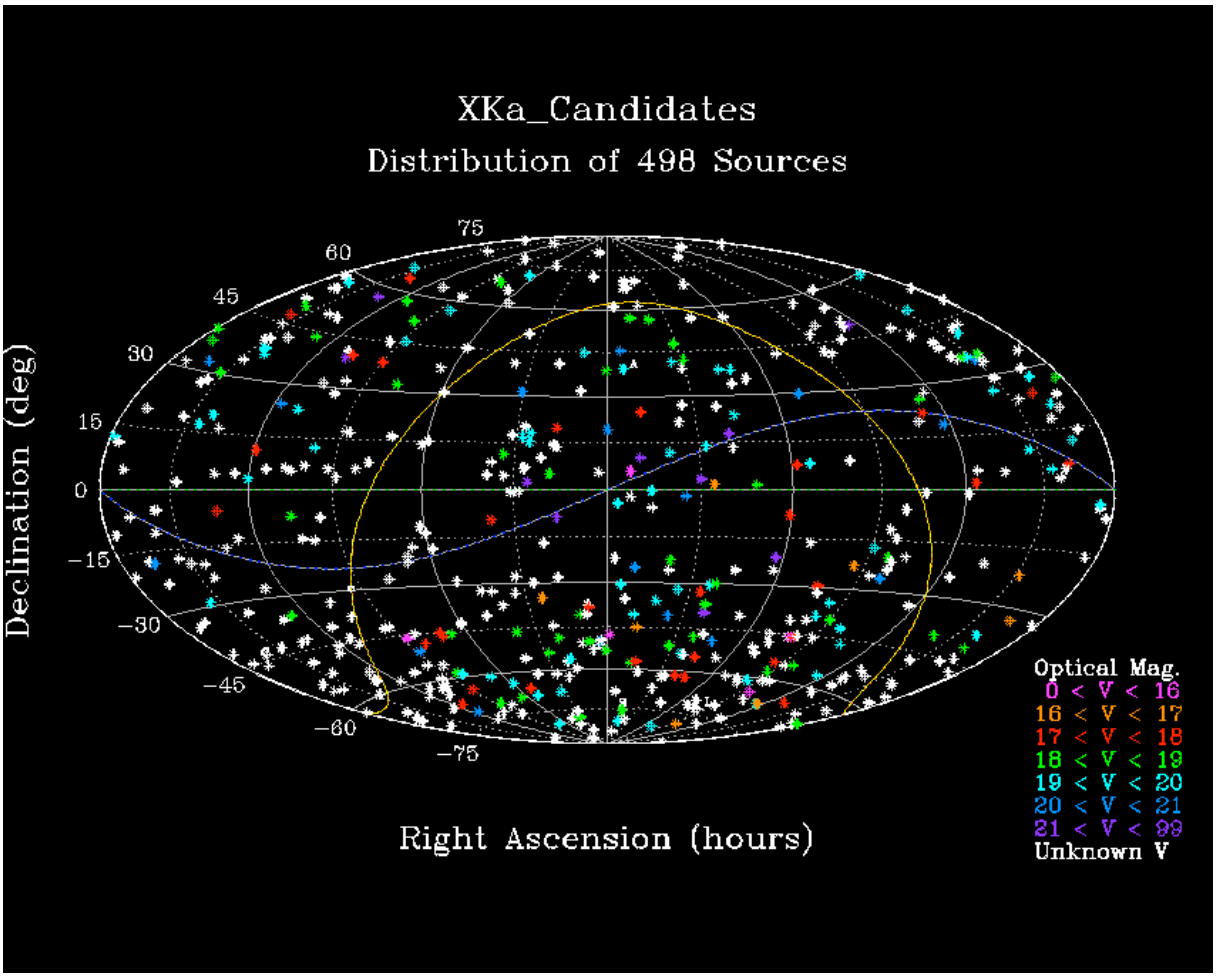

Fig. 4 Candidates for X/Ka VLBI observations chosen on the basis of at least 200 mJy of compact X-band flux where compact is defined as 70% of the flux in an unresolved core (Sotuela et al, 2011). Note the rich set of candidates in the southern polar cap.